Article

Comparison of Analytical Techniques for Purity Evaluation of Single-Walled Carbon Nanotubes

Mikhail E. Itkis, Daniel E. Perea, Richard Jung, Sandip Niyogi, and Robert C. Haddon

J. Am. Chem. Soc., **2005**, 127 (10), 3439-3448• DOI: 10.1021/ja043061w • Publication Date (Web): 19 February 2005

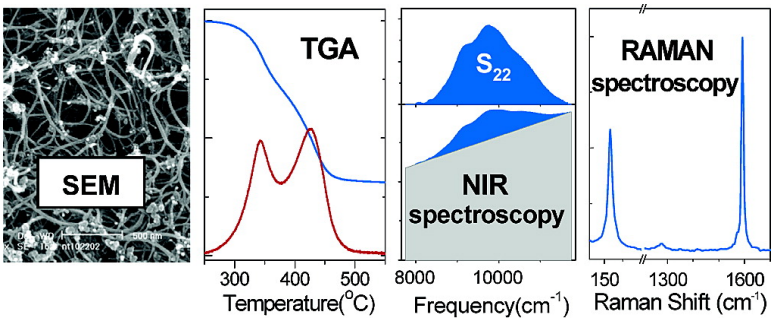

More About This Article

Additional resources and features associated with this article are available within the HTML version:

- Supporting Information
- Links to the 26 articles that cite this article, as of the time of this article download
- Access to high resolution figures
- Links to articles and content related to this article
- Copyright permission to reproduce figures and/or text from this article

View the Full Text HTML

J|A|C|S
ARTICLES
Published on Web 02/19/2005

Comparison of Analytical Techniques for Purity Evaluation of Single-Walled Carbon Nanotubes

Mikhail E. Itkis,[†] Daniel E. Perea,[‡] Richard Jung,[†] Sandip Niyogi,[†] and Robert C. Haddon*,[†]

Contribution from the Center for Nanoscale Science and Engineering, Departments of Chemistry and Chemical & Environmental Engineering, University of California, Riverside, California 92521-0403, and Carbon Solutions, Inc., Riverside, California 92506

Received November 17, 2004; E-mail: haddon@ucr.edu

Abstract: We compare popular analytical techniques, including scanning and transmission electron microscopy (SEM and TEM), thermogravimetric analysis (TGA), and Raman and near-infrared (NIR) spectroscopy, for the evaluation of the purity of bulk quantities of single-walled carbon nanotubes (SWNTs). Despite their importance as imaging techniques, SEM and TEM are not capable of quantitatively evaluating the purity of typical inhomogeneous bulk SWNT samples because the image frame visualizes less than 1 pg of SWNT material; furthermore, there is no published algorithm to convert such images into numerical data. The TGA technique is capable of measuring the amount of metal catalyst in an SWNT sample, but does not provide an unambiguous separation between the content of SWNTs and carbonaceous impurities. We discuss the utilization of solution-phase near-infrared spectroscopy and solution-phase Raman spectroscopy to quantitatively compare arbitrary samples of bulk SWNT materials of different purities. The primary goal of this paper is to provide the chemical community with a realistic evaluation of current analytical tools for the purity evaluation of a bulk sample of SWNTs. The secondary goal is to draw attention to the growing crisis in the SWNT industry as a result of the lack of quality control and the misleading advertising by suppliers of this material.

1. Introduction

Single-walled carbon nanotubes (SWNTs) are the most promising of all nanomaterials, with unique electronic and mechanical properties which lend themselves to a variety of applications, such as field-emission displays,[1] nanostructured composite materials,[2] nanoscale sensors,[3] and elements of new nanoscale logic circuits.[4,5] In all cases the quality of the SWNT material is important, and for some applications it is paramount. Despite sustained efforts, all currently known SWNT synthetic techniques[5−14] generate significant quantities of impurities, such as amorphous and graphitic forms of carbon and carbon-encapsulated catalytic metal nanoparticles.[12,13,15,16] The presence of such impurities necessitates the application of vigorous purification procedures,[10,17−21] which adds to the high cost of production and limits the application of these materials.

The quality and yield of SWNTs in any given production method depend on a number of factors, such as the temperature field and pressure in the reaction zone, the composition of catalysts utilized, the type and flow rate of buffer gas, and many other parameters which are specific to the particular synthetic techniques.[5,7−11,14,22−24] The optimization of the SWNT syn-

[†] University of California.
[‡] Carbon Solutions, Inc.

(1) Zhou, O.; Shimoda, H.; Gao, B.; Oh, S.; Fleming, L.; Yue, G. *Acc. Chem. Res.* **2002**, *35*, 1045−1053.
(2) Mamedov, A. F.; Kotov, N. A.; Prato, M.; Guldi, D. M.; Wicksted, J. P.; Hirsch, A. *Nat. Mater.* **2002**, *1*, 190−194.
(3) Kong, J.; Franklin, N. R.; Zhou, C.; Chapline, M. G.; Peng, S.; Cho, K.; Dai, H. *Science* **2000**, *287*, 622−625.
(4) Avouris, P. *Acc. Chem. Res.* **2002**, *35*, 1026−1034.
(5) Dai, H. *Acc. Chem. Res.* **2002**, *35*, 1035−1044.
(6) Iijima, S.; Ichihashi, T. *Nature* **1993**, *363*, 603−605.
(7) Bethune, D. S.; Kiang, C. H.; de Vries, M. S.; Gorman, G.; Savoy, R.; Vazquez, J.; Bevers, R. *Nature* **1993**, *363*, 605−607.
(8) Guo, T.; Nikolaev, P.; Thess, A.; Colbert, D. T.; Smalley, R. E. *Chem. Phys. Lett.* **1995**, *243*, 49−54.
(9) Journet, C.; Maser, W. K.; Bernier, P.; Loiseau, A.; Lamy de la Chappelle, M.; Lefrant, S.; Deniard, P.; Lee, R.; Fischer, J. E. *Nature* **1997**, *388*, 756−758.
(10) Rinzler, A. G.; Liu, J.; Dai, H.; Nilolaev, P.; Huffman, C. B.; Rodriguez-Macias, F. J.; Boul, P. J.; Lu, A. H.; Heymann, D.; Colbert, D. T.; Lee, R. S.; Fischer, J. E.; Rao, A. M.; Eklund, P. C.; Smalley, R. E. *Appl. Phys. A* **1998**, *67*, 29−37.
(11) Nikolaev, P.; Bronikowski, M. J.; Bradley, R. K.; Rohmund, F.; Colbert, D. T.; Smith, K. A.; Smalley, R. E. *Chem. Phys. Lett.* **1999**, *313*, 91−97.
(12) Bethune, D. S. *Physica B* **2002**, *323*, 90−96.
(13) Itkis, M. E.; Perea, D.; Niyogi, S.; Rickard, S.; Hamon, M.; Hu, H.; Zhao, B.; Haddon, R. C. *Nano Lett.* **2003**, *3*, 309−314.
(14) Itkis, M. E.; Perea, D.; Niyogi, S.; Love, J.; Tang, J.; Yu, A.; Kang, C.; Jung, R.; Haddon, R. C. *J. Phys. Chem. B* **2004**, *108*, 12770−12775.
(15) Yudasaka, M.; Komatsu, J.; Ichihashi, T.; Achiba, Y.; Iijima, S. *J. Phys. Chem.* **1998**, *102*, 4892−4896.
(16) Yudasaka, M.; Sensui, N.; Takizawa, M.; Bandow, S.; Ichihashi, T.; Iijima, S. *Chem. Phys. Lett.* **1999**, *312*, 155−160.
(17) Dillon, A. C.; Gennett, T.; Jones, K. M.; Alleman, J. L.; Parilla, P. A.; Heben, M. J. *Adv. Mater.* **1999**, *11*, 1354−1358.
(18) Dillon, A. C.; Gennett, T.; Parilla, P. A.; Alleman, J. L.; Jones, K. M.; Heben, M. J. *Mater. Res. Soc. Symp. Proc.* **2001**, *633*, A5.2.1−A5.2.6.
(19) Gorelik, O. P.; Nikolaev, P.; Arepalli, S. NASA contractor report CR-2000-208926; 2001.
(20) Hu, H.; Zhao, B.; Itkis, M. E.; Haddon, R. C. *J. Phys. Chem. B* **2003**, *107*, 13838−13842.
(21) Haddon, R. C.; Sippel, J.; Rinzler, A. G.; Papadimitrakopoulos, F. *MRS Bull.* **2004**, *29*, 252−259.
(22) Yudasaka, M.; Kikuchi, R.; Ohki, Y.; Ota, E.; Yoshimura, S. *Appl. Phys. Lett.* **1997**, *70*, 1817−1818.
(23) Journet, C.; Bernier, P. *Appl. Phys. A* **1998**, *67*, 1−9.
(24) Saito, Y.; Tani, Y.; Miyagawa, N.; Mitsushima, K.; Kasuya, A.; Nishina, Y. *Chem. Phys. Lett.* **1998**, *294*, 593−598.

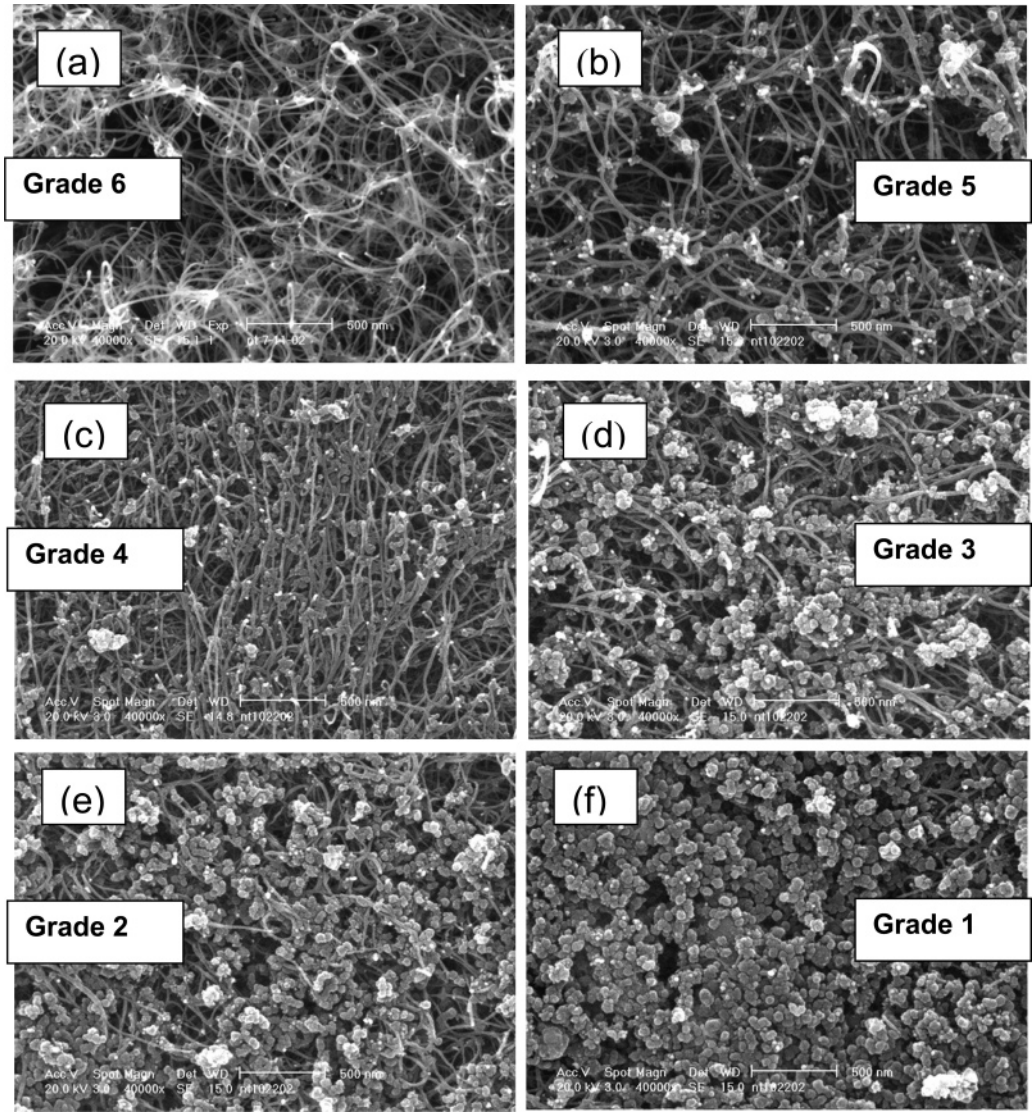

Figure 1. SEM purity grading system showing highest purity grade 6 to lowest grade 1 samples obtained from SEM images of AP-SWNT soot produced by the electric arc discharge technique. Note that images b−f (grades 5−1) were obtained from samples taken from the same synthetic experiment.

thesis, as well as subsequent purification steps, is a multiparametric task which requires the accurate and efficient evaluation of small changes in the quality and yield of bulk quantities of the SWNT product as a function of the synthetic parameters and purification protocol. Ideally, such a procedure should provide a rapid, convenient, and unambiguous measure of the bulk purity of standard SWNT samples with instrumentation that is routinely available in research laboratories. In this paper we compare the capabilities of different analytical techniques, such as scanning and transmission electron microscopy (SEM and TEM), thermogravimetric analysis (TGA), and Raman and near-infrared (NIR) spectroscopy, for the evaluation of the purity of bulk quantities of SWNT samples.

While the reader may believe that this is a settled issue because many suppliers label their SWNT products with percentage purities, we have evaluated many such samples and found the majority to be overstated—some to a high degree.[25] Progress in chemistry and material science has been marked by the ability to obtain pure substances: the isolation of the pure elements and the refinements that have occurred in electronics-grade silicon are obvious examples. While it may not be possible to obtain analytically pure SWNTs, it is high time for the SWNT industry to make a serious attempt to divulge to its customers the quality of the products that are offered for commercial sale. In this paper we attempt to delineate the best metrics for this discourse in the hope that quality control and quality assurance may take hold in the SWNT community.

2. Scanning Electron Microscopy

TEM and SEM have traditionally been the most important techniques for the characterization of carbon nanotubes. Indeed, SWNTs were discovered in 1993 using TEM,[6,7] and high-resolution TEM remains a major analytical tool for the study of SWNT nucleation and growth.[26−28] The SEM technique has been extensively used to monitor the efficiency of the bulk-scale production of SWNTs by a variety of synthetic tech-

(25) Giles, J. *Nature* **2004**, *432*, 791.

(26) Gavillet, J.; Loiseau, A.; Ducastelle, F.; Thair, S.; Bernier, P.; Stephan, O.; Thibault, J.; Charlier, J. C. *Carbon* **2002**, *40*, 1649−1663.

(27) Loiseau, A.; Gavillet, J.; Ducastelle, F.; Thibault, J.; Stephan, O.; Bernier, P.; Thair, S. *C. R. Phys.* **2003**, *4*, 975−991.

(28) Gavillet, J.; Thibault, J.; Stephan, O.; Amara, H.; Loiseau, A.; Bichara, C.; Gaspard, J.; Ducastelle, F. *J. Nanosci. Nanotechnol.* **2004**, *4*, 346−359.

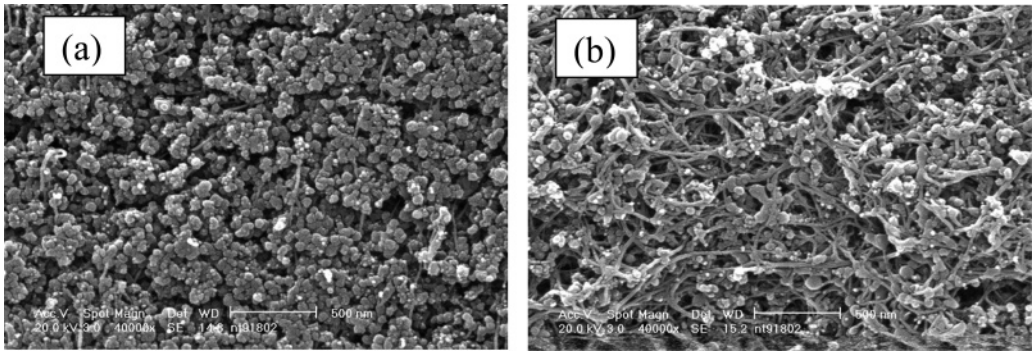

Figure 2. SEM images of SWNT soot of similar quality, but different apparent purity as a result of differences in the sample preparation procedure: (a) unprocessed dry powder sample, apparent grade 1; (b) the sample was dispersed in DMF before being placed on the SEM holder and drying, apparent grade 2−3.

niques,[9−11] and it has traditionally been the most popular tool to evaluate the quality of as-prepared SWNT soot (AP-SWNT). Beginning in 1998, SEM was our preferred technique for optimizing the electric arc discharge (EA) synthesis of SWNTs, and we describe our observations below.

Figure 1 shows SEM images of EA-AP-SWNT soot collected directly from the arc chamber. These images represent a fairly typical distribution of the quality of SWNT soot, which can be observed within a production run (Figure 1) with fixed reaction parameters.[13,14] To assess the bulk purity of an AP-SWNT batch with this degree of inhomogeneity, multiple SEM frames must be evaluated and averaged over a sufficiently broad sample to provide meaningful statistics. To facilitate the evaluation of the images, we developed a visual grading scale running from 1 (lowest purity) to 6 (highest purity), and produced a library of SEM images which we assigned to each grade by visual inspection (Figure 1).

On the basis of this analysis, the grade 6 material (Figure 1a) was assigned a purity of 85−100%, grade 5 (Figure 1b) 65−85%, grade 4 (Figure 1c) 50−65%, grade 3 (Figure 1d) 30−50%, grade 2 (Figure 1e) 15−30%, and grade 1 (Figure 1f) 5−15%. It is important to note that we attempted to expand this scheme to encompass 10 grades as we believed that this would be more acceptable to the community, but we could never convince ourselves that it was possible to achieve this degree of visual resolution. With this grading system in place we were able to complete the purity assessment of each 10−20 g batch of AP-SWNTs in 2−3 h of SEM time, by interpreting the images in real time on the SEM screen.

We found several drawbacks to this grading system that were mainly associated with the application of the SEM technique to the evaluation of bulk SWNT samples. The EA-AP-SWNT soot (including grade 6, Figure 1a) contains about 30% metal catalyst, which is invisible to SEM, but easily observed by TEM or in TGA measurements. Thus, the absolute weight purity of grade 6 SWNTs does not exceed 70%. Furthermore, a thin coating of amorphous carbon on the SWNTs is invisible to the SEM technique. In addition, we found that grading by visual inspection of SEM frames depended on the method of sample preparation. To illustrate this point, we show in Figure 2a an SEM image of an SWNT sample placed on the carbon tape attached to the SEM holder in the form of a dry powder, and in Figure 2b an image of the same fragment of SWNT soot which was initially dispersed in *N*,*N*-dimethylformamide (DMF) by ultrasonication before being dropped on the carbon tape.

The image field of the dry powder sample (Figure 2a) consists almost solely of aggregates of amorphous carbon and nanoparticles with very few SWNTs, and this sample would correspond to grade 1 (Figure 1f) of the SEM library. Dispersal of the same sample in DMF (Figure 2b) reveals a higher density of SWNTs and corresponds to a grade between 3 and 2 (Figure 1d,e). We found that the apparent increase in the purity of AP-SWNT soot on dispersion is fairly typical in SEM analysis. Ultrasonication in DMF breaks and disperses the aggregates of amorphous carbon and nanoparticles and leaves the material in the form of a thin coating on the walls of the SWNT bundles, and this leads to the illusion of increased purity (Figure 2b).

A more serious drawback of the microscopic techniques is the scale of the TEM and SEM analyses. We estimate that the amount of material that is apparent in a typical SEM frame (Figures 1 and 2) is less than 10^{-12} g.[13] It is impossible to homogenize AP-SWNTs so that a 10^{-12} g surface sample will be representative of a 10 g batch of material. Even at the 10^{-10} g level (for a practical limit of 100 SEM frames per batch), it is impossible to achieve a quantitative and statistically significant assessment of the bulk purity of a batch of SWNTs in a reasonable amount of time. Furthermore, the assignments of grades and purities to the library given in Figure 1 is highly subjective, and we could not obtain reproducible opinions of the purity of samples among different members of our research group with this methodology. Nevertheless, we do not dispute the attraction of SEM images of impurity-free SWNTs, and the SEM technique provides a necessary and useful visual confirmation of the quality of high-purity samples.[10,17−19,21,29]

3. Near-Infrared Spectroscopy

Thin film transmission NIR spectroscopy has been used to detect SWNT interband transitions,[30−35] to evaluate the effect of ionic (doping) and covalent chemistry on the band structure,[32,36−40] to compare the abundance and diameter distribution of the SWNTs produced by laser vaporization as a function of furnace temperature and Co/Ni catalyst composition,[41,42] and to monitor the efficiency of purification.[43] Dissolution of the SWNTs by end-group functionalization allowed us to monitor the SWNT interband transitions and their modification due to chemical processing and doping in the solution phase.[40,44−46]

Recently we proposed a quantitative procedure to assess the relative carbonaceous purity of bulk quantities of AP-SWNT

(29) Arepalli, S.; Nikolaev, P.; Gorelik, O. P.; Nadjiev, V. G.; Holmes, W.; Files, B.; Yowell, L. *Carbon* **2004**, *42*, 1783−1791.

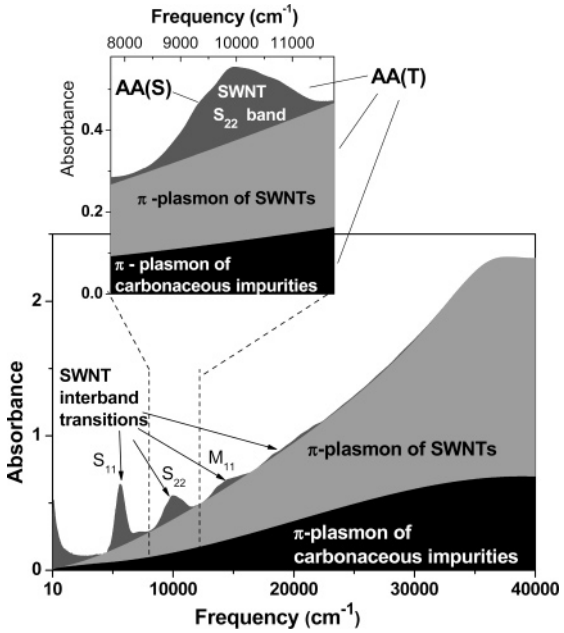

Figure 3. Schematic illustration of the electronic spectrum of a typical SWNT sample produced by the electric arc method. The inset shows the region of the S_{22} interband transition utilized for NIR purity evaluation. In the diagram, AA(S) = area of the S_{22} spectral band after linear baseline correction and AA(T) = total area of the S_{22} band including SWNT and carbonaceous impurity contributions. The NIR relative purity is given by RP = (AA(S)/AA(T))/0.141 (see the text).

soot on the basis of solution (dispersion) phase NIR spectroscopy.[13,21,47] Figure 3 shows a schematic of the absorption spectrum of an arbitrary EA-produced SWNT sample in the spectral range between the far-IR and the UV (10−45000 cm^{-1}),[21,32] with the absorptions due to SWNTs and carbonaceous impurities shown in different colors to illustrate the spectral components (although it is not yet possible to analytically separate these contributions).[47] The high-energy part of the spectrum is dominated by the π-plasmon absorption from both SWNTs and carbonaceous impurities, and the tail of this peak extends into the far-IR part of the spectrum. The NIR−visible part of the spectrum from 4000 to 17000 cm^{-1} exhibits characteristic absorption features, originating from the interband transitions in semiconducting and metallic SWNTs, which ride on the top of the π-plasmon tail. It is intuitively understandable that the strength of these characteristic features in comparison with the featureless baseline provides a measure of the purity of the SWNT material.

While the S_{11} transition is the most prominent, we chose the second semiconducting transition (S_{22}, inset to Figure 3) for the purity evaluation[13,21,47] because the S_{22} transition is less susceptible to incidental doping and because it matches the transmission window for DMF which is utilized for the solution (dispersion) phase NIR spectroscopy. It is known that DMF is one of the most efficient solvents for dispersing both raw and purified SWNT material,[48,49] and we have found that DMF can partially compensate the incidental doping affecting the S_{22} interband transition.

For accurate evaluation of bulk quantities of SWNT material (>10 g), special attention must be paid to the preparation of the NIR samples.[13,21,47] In the first step, the material is mechanically homogenized to give a dry powder; 50 mg of this powder is then dispersed in 100 mL of DMF by use of an ultrasonic bath in combination with 10 min of mechanical stirring to yield a homogeneous slurry. Following 2−3 dilution−ultrasonication steps at the 10 mL level, this procedure gives rise to a semitransparent, visually nonscattering dispersion with optical density 0.2 ± 0.05 in a 10 mm path length cuvette at a frequency of 11750 cm^{-1}, which corresponds to an SWNT concentration ≅0.01 mg/mL.[13,47] This solution-phase homogenization procedure reproducibly generates an SWNT sample which is representative of the quality of the bulk (see below).

We have identified the ratio AA(S)/AA(T) as the simplest possible metric of SWNT purity, where AA(S) is the area of the S_{22} interband transition after linear baseline subtraction (dark gray area in the inset to Figure 3) and AA(T) is the total area under the spectral curve, with both areas taken between the spectral cutoffs of 7750 and 11750 cm^{-1}, which were chosen to capture the S_{22} interband electronic transitions of SWNTs of the diameter produced by the EA process with Ni/Y catalysts.[13,21,47] This ratio is then normalized by dividing by 0.141, the value of AA(S)/AA(T) obtained for an arbitrary high-purity reference sample of AP-SWNTs (denoted R2),[13,21,47] and this procedure therefore gives rise to a relative purity (RP). Because a 100% pure reference sample is not currently available, it is not possible to give an absolute determination of SWNT purity, although progress may be noted.[47] Nevertheless, through the joint efforts of the carbon nanotube community, and with sample exchanges between research groups, it will be possible to further refine the choice of a reference sample and to asymptotically converge on a standard for the measurement of absolute purity.

(30) Kataura, H.; Kumazawa, Y.; Maniwa, Y.; Umezu, I.; Suzuki, S.; Ohtsuka, Y.; Achiba, Y. *Synth. Met.* **1999**, *103*, 2555−2558.
(31) Petit, P.; Mathis, C.; Journet, C.; Bernier, P. *Chem. Phys. Lett.* **1999**, *305*, 370−374.
(32) Itkis, M. E.; Niyogi, S.; Meng, M.; Hamon, M.; Hu, H.; Haddon, R. C. *Nano Lett.* **2002**, *2*, 155−159.
(33) Hennrich, F.; Lebedkin, S.; Malik, S.; Tracy, J.; Barczewski, M.; Rosner, H.; Kappes, M. *Phys. Chem. Chem. Phys.* **2002**, *4*, 2273−2277.
(34) Hamon, M. A.; Itkis, M. E.; Niyogi, S.; Alvaraez, T.; Kuper, C.; Menon, M.; Haddon, R. C. *J. Am. Chem. Soc.* **2001**, *123*, 11292−11293.
(35) Wu, Z.; Chen, Z.; Du, X.; Logan, J. M.; Sippel, J.; Nikolou, M.; Kamaras, K.; Reynolds, J. R.; Tanner, D. B.; Hebard, A. F.; Rinzler, A. G. *Science* **2004**, *305*, 1273−1276.
(36) Kazaoui, S.; Minami, N.; Jacquemin, R.; Kataura, H.; Achiba, Y. *Phys. Rev. B* **1999**, *60*, 13339−13342.
(37) Kazaoui, S.; Minami, N.; Matsuda, N.; Kataura, H.; Achiba, Y. *Appl. Phys. Lett.* **2001**, *78*, 3433−3435.
(38) Hennrich, F.; Wellmann, R.; Malik, S.; Lebedkin, S.; Kappes, M. M. *Phys. Chem. Chem. Phys.* **2003**, *5*, 178−183.
(39) Kamaras, K.; Itkis, M. E.; Hu, H.; Zhao, B.; Haddon, R. C. *Science* **2003**, *301*, 1501.
(40) Hu, H.; Zhao, B.; Hamon, M. A.; Kamaras, K.; Itkis, M. E.; Haddon, R. C. *J. Am. Chem. Soc.* **2003**, *125*, 14893−14900.
(41) Jost, O.; Gorbunov, A. A.; Pompe, W.; Pichler, T.; Friedlein, R.; Knupfer, M.; Reibold, M.; Bauer, H.-D.; Dunsch, L.; Golden, M. S.; Fink, J. *Appl. Phys. Lett.* **1999**, *75*, 2217−2219.
(42) Jost, O.; Gorbunov, A. A.; Moller, J.; Pompe, W.; Lui, X.; Georgi, P.; Dunsch, L.; Golden, M. S.; Fink, J. *J. Phys. Chem. B* **2002**, *106*, 2875−2883.
(43) Sen, R.; Rickard, S. M.; Itkis, M. E.; Haddon, R. C. *Chem. Mater.* **2003**, *15*, 4273−4279.
(44) Chen, J.; Hamon, M. A.; Hu, H.; Chen, Y.; Rao, A. M.; Eklund, P. C.; Haddon, R. C. *Science* **1998**, *282*, 95−98.
(45) Chen, J.; Rao, A. M.; Lyuksyutov, S.; Itkis, M. E.; Hamon, M. A.; Hu, H.; Cohn, R. W.; Eklund, P. W.; Colbert, D. T.; Smalley, R. E.; Haddon, R. C. *J. Phys. Chem. B* **2001**, *105*, 2525−2528.
(46) Niyogi, S.; Hamon, M. A.; Hu, H.; Zhao, B.; Bhowmik, P.; Sen, R.; Itkis, M. E.; Haddon, R. C. *Acc. Chem. Res.* **2002**, *35*, 1105−1113.
(47) Zhao, B.; Itkis, M. E.; Niyogi, S.; Hu, H.; Zhang, J.; Haddon, R. C. *J. Phys. Chem. B* **2004**, *108*, 8136−8141.
(48) Liu, J.; Casavant, M. J.; Cox, M.; Walters, D. A.; Boul, P.; Lu, W.; Rimberg, A. J.; Smith, K. A.; Colbert, D. T.; Smalley, R. E. *Chem. Phys. Lett.* **1999**, *303*, 125−129.
(49) Niyogi, S.; Hamon, M. A.; Perea, D.; Kang, C. B.; Zhao, B.; Pal, S. K.; Wyant, A. E.; Itkis, M. E.; Haddon, R. C. *J. Phys. Chem. B* **2003**, *107*, 8799−8804.

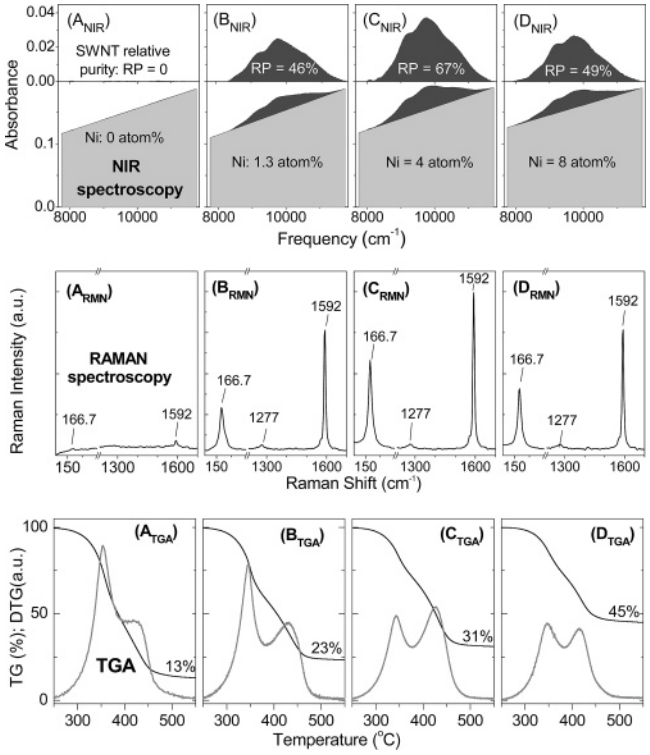

Figure 4. Solution-phase NIR (top panel) and Raman (middle panel) spectra, and TGA data (bottom panel) for four SWNT samples, A−D, produced by the electric arc discharge technique using Ni catalyst concentrations of 0, 1.3, 4, and 8 atom %, with a constant yttrium catalyst concentration of 1 atom %. The NIR panel (A_{NIR}−D_{NIR}) shows the area of the S_{22} feature (dark shading, top part) and complete area (bottom part) used for purity calculations. A degree of correlation between the data obtained from the different analytical techniques is apparent (see the text).

To allow for SWNTs of different diameters, the purity evaluation procedure can be modified by adjusting the spectral cutoffs.[47]

The top panel in Figure 4 illustrates the use of the NIR-based purity evaluation technique for the study of the effect of Ni/Y catalyst composition on the large-scale electric arc discharge production of SWNTs.[14] The solution-phase NIR absorption spectra in the range of the S_{22} interband transitions are shown for a set of SWNT samples synthesized with Ni concentrations between 0 and 8 atom % at a constant Y concentration of 1 atom %. The other panels of Figure 4 show Raman and TGA data obtained from the same set of SWNT samples and are discussed below.

The top panel of Figure 4 shows the strong dependence of the area of the S_{22} feature (dark shading) on the concentration of Ni in the catalyst. The RP of the AP-SWNTs is proportional to the ratio of the spectral area of the S_{22} interband transition to the total area under the spectral curve (Figure 4, top panel), and clearly reaches a maximum in the vicinity of a Ni concentration of 4 atom % in agreement with the original finding.[9] Thus, the NIR technique provides an efficient tool to analytically evaluate the effect of the concentration of Ni catalyst on the purity of the AP-SWNT product.[14]

The NIR purity evaluation method depends on the absorption of light, but the interaction of electromagnetic radiation with SWNTs may lead to scattering.[21] The occurrence of light scattering would be a complicating factor in the interpretation of the absorption spectra of SWNTs and might affect the accuracy of the purity evaluation by contributing to the level

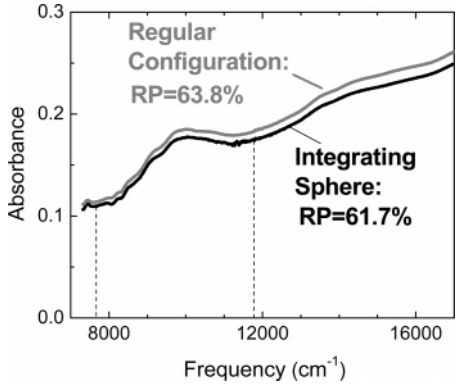

Figure 5. Solution-phase absorption spectra of an SWNT sample in regular transmission configuration (gray curve) and using an integrating sphere (black curve) to collect the scattered light.

Table 1. NIR Purity (%) in Regular and Integrating Sphere Configuration

	sample 1	sample 2	sample 3
regular config	20.5	38.5	63.8
integrating sphere config	16.5	35.5	61.7

of the baseline (Figures 3 and 4), thus reducing the measured purity. The spectral contribution to light scattering (S) is controlled by the ratio of the characteristic dimension of the scattering particles (d) and the wavelength of the incident light (λ). In the present situation, we consider the SWNT length to be the characteristic dimension d, because the strongest interaction of light with SWNTs occurs when the light is polarized along the SWNT axis. Most SWNT samples show a wide length distribution, which is typically concentrated in the range $d = 0.5-3\ \mu$m, and this is comparable with the wavelength of light in the vicinity of the S_{22} interband transition ($\lambda \approx 1\ \mu$m) that is utilized for purity evaluation. In this circumstance ($d \approx \lambda$) Mie scattering is expected to dominate,[21] and this scattering mechanism becomes more important as the particle size increases ($d > \lambda$). In the spectral range of interest there is a crossover between $\lambda > d$ and $\lambda < d$, and this makes it difficult to theoretically estimate the influence of scattering on the NIR absorption spectra, especially in the case of SWNT solution samples which present themselves to the light beam as an ensemble of dynamic highly anisotropic particles.

To experimentally address these questions, we made use of an integrating sphere in the sample compartment of the Cary 500 UV−vis−NIR spectrophotometer utilized in our experiments, as discussed previously.[50] The integrating sphere should recover a significant fraction of the scattered light normally lost in a standard transmission configuration with a narrow aperture of collection. Figure 5 shows the NIR absorption spectra of an AP-SWNT dispersion in DMF measured with regular and integrating sphere configurations for the collection of light. The introduction of the integrating sphere collection leads to a small decrease in the level of the baseline, and the calculated relative purites were found to be 63.8% in regular and 61.7% in the integrating sphere configurations; Table 1 shows a comparison for three AP-SWNT samples with relative purities between 20% and 60%.

If scattering were to be significant, we would expect a reduction in the relative purity, when measured in the regular

(50) Lebedkin, S.; Hennrich, F.; Skipa, T.; Kappes, M. *J. Phys. Chem. B* **2003**, *107*, 1949−1956.

configuration, in comparison with the case of the integrating sphere technique. Table 1 shows the opposite trend, with a lower measured relative purity in the integrating sphere configuration, although the deviations are within the experimental accuracy of our technique.[13] This suggests that, in the case of properly dispersed SWNTs, scattering does not materially affect the NIR relative purity evaluation. Incompletely dispersed samples with large aggregates of SWNTs would be expected to affect the purity evaluation as a result of Mie scattering, and it was for this reason that we emphasized the importance of the sample preparation procedure[13] and stressed the necessity of utilizing low SWNT solution concentrations ($\leq$0.01 mg/mL). It proved to be more difficult to control scattering in the case of SWNT thin films, and this was one factor which led to our choice of solution-phase[13,21,47] rather than thin film[32,41] transmission spectroscopy for the relative purity evaluation studies.

4. Thermogravimetric Analysis

Thermogravimetric analysis is a widely used analytical technique for the determination of the amount of metal catalyst in SWNT samples.[17,18,29,51] The relative amount of different fractions in AP-SWNT soot can be identified if their combustion temperatures are well separated, and TGA data have been analyzed in terms of SWNTs, amorphous carbon, and graphitic nanoparticles.[51] A typical TGA experiment makes use of 1−5 mg of material, which is at the level 0.01% of the total amount of AP-SWNT soot produced in a bulk preparation, so it is imperative that proper homogenization is achieved to obtain representative test samples.[13] In our TGA experiments, we adopted a solution (dispersion) phase homogenization procedure similar to that used for the NIR purity evaluation.[13] However, after the first dispersion−homogenization step the highly concentrated DMF slurry of AP-SWNT soot was dried to produce a dense homogeneous sample.

Figure 4 (bottom panel) shows the results of TGA experiments run in air at a heating rate of 5 °C/min, conducted on the same four SWNT samples previously discussed in connection with the NIR spectroscopy (top panel of Figure 4). The derivative data show two peaks in the vicinity of 350 and 420 °C. The low-temperature peak is usually associated with amorphous carbon and the high-temperature peak is considered to originate from the SWNT fraction,[17,18,29,51] and we tentatively adopt this assignment in an effort to compare the TGA and NIR results. The fraction of metal catalyst (M) may be obtained by measuring the TGA residue after ramping of the sample temperature to 1000 °C. As a result of oxide formation the weight of residue should be reduced by 20% to account for the oxygen content of the pyrolysis products.[20] The availability of data on the relative contributions of these three major fractions would allow an accurate estimation of the absolute purity of the SWNT soot. The results in Figure 4 show that there is a certain degree of correlation between the NIR and the TGA data. The integral of the first peak in the derivative data near 350 °C decreases, while the amplitude of the peak near 420 °C increases from sample A to sample C, as the Ni concentration increases from 0 to 4 atom %, in qualitative agreement with the NIR data. Furthermore, both the TGA and NIR data show a decline in the SWNT content for sample D at a Ni concentration of 8 atom % (D_{NIR} and D_{TGA}).

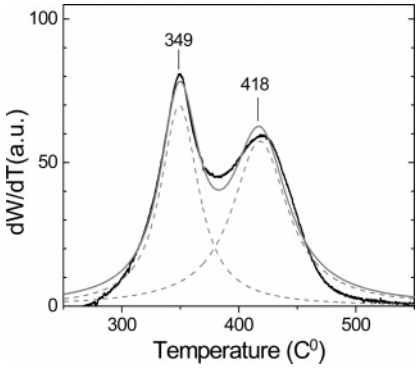

Figure 6. Experimental TGA derivative curve (black line) and best fit (gray solid line) using two Lorentzian curves (dashed lines).

Nevertheless, we found it very difficult to extract quantitative data from the TGA measurements. Figure 6 demonstrates an attempt to fit the experimental derivative data using two Lorentzians, in the hope that the low-energy Lorentzian would represent the contribution due to amorphous carbon and the high-energy peak could be assigned to the SWNTs. We observed significant deviations of the best fit curve from the experimental data (Figure 6), which was especially noticeable at the wings of the derivative curve (below 300 °C and above 450 °C) and around each extremum. We found that it would require at least four Lorentzian components with no clear physical interpretation to adequately describe the temperature dependence of the derivative data in Figure 6. In some cases Gaussian fitting provides a more satisfactory match to the experimental data in the high-temperature range, but we were unable to achieve complete deconvolution of the experimental curves using two Gaussian components.

Reference to Figure 4 (A_{TGA}) shows that sample A, which was produced without Ni catalyst, gives a TGA profile with a significant presence of the high-temperature component that is usually associated with SWNTs in the AP-SWNT soot. It is known that Y alone is not a useful catalyst for the production of SWNTs,[9,16,23,28,52] and this is confirmed by the NIR data [Figure 4 (A_{NIR})].[14] The Raman spectrum obtained for sample A in the middle panel of Figure 4 (A_{RMN}) revealed only trace amounts of SWNTs. Thus, the peak in the TGA data at 420 °C is not uniquely associated with SWNTs, and there are apparently other forms of carbon that have similar combustion temperatures. Thus, in the TGA experiments the AP-SWNT soot behaves as a heterogeneous mixture of unresolved multiple components with a wide distribution of combustion temperatures. In addition, the interpretation of the results is further complicated by the exothermic metal oxidation reaction and the dependence of the TGA results on the temperature ramp rate.[14,29]

5. Raman Spectroscopy. Comparison of Raman and NIR Spectroscopy for Purity Evaluation

The Raman scattering from SWNTs is resonantly enhanced if the excitation energy matches the separations between the pairs of Van Hove singularities in the one-dimensional electronic density of states of the SWNTs.[53−55] The two most prominent features observed in the first-order resonant Raman spectrum of the SWNTs are the low-frequency radial breathing mode

(51) Zhang, M.; Yudasaka, M.; Koshio, A.; Iijima, S. *Chem. Phys. Lett.* **2002**, *364*, 420−426.

(52) Takizawa, M.; Bandow, S.; Yudasaka, M.; Ando, Y.; Shimoyama, H.; Iijima, S. *Chem. Phys. Lett.* **2000**, *326*, 351−357.

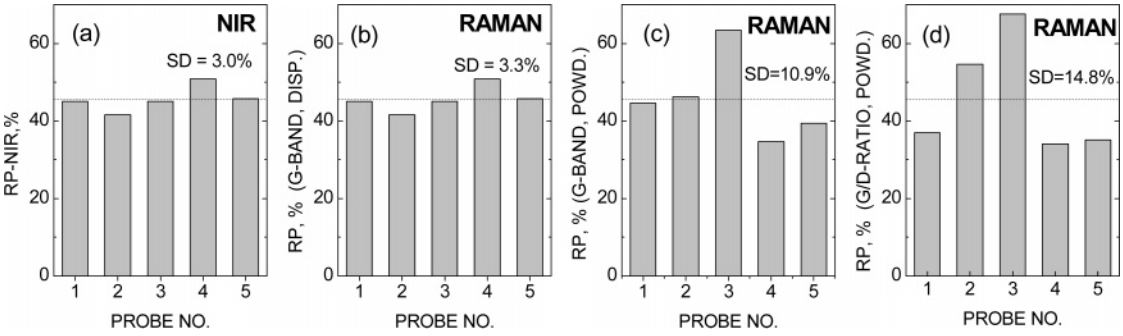

Figure 7. Reproducibility test of purity evaluation techniques using NIR and Raman spectroscopy, in which five 50 mg probe samples were obtained from the same 10 g mechanically homogenized batch of AP-SWNT soot: (a) solution-phase NIR purity, average purity 46%, SD = 3%; (b) solution-phase Raman spectroscopy, G-band area, SD = 3.3%; (c) solid-phase Raman spectroscopy, G-band area, SD = 10.9%; (d) solid-phase Raman spectroscopy, ratio of the G-band and D-band areas, SD = 14.8%. The data in (b)−(d) were normalized to the average purity obtained from the NIR results (RP = 46%).

(RBM) located typically in the range 100−300 cm^{-1} and the high-frequency G-band between 1500 and 1600 cm^{-1}, which is composed of several tangential modes due to stretching vibrations of the SWNT sidewall carbon−carbon bonds.[53−55] Both of these features are apparent in the Raman spectra shown in the middle panel of Figure 4. The RBM frequency can be used to determine the diameter of the SWNTs present in the sample, and the spectral shape of the G-band can be used to distinguish between metallic and semiconducting SWNTs.[52−55] The intensities of both RBM- and G-bands were used to attempt the evaluation of the SWNT content in AP-SWNT soot, by use of Raman spectroscopy.[17,18,23,52,56] Also seen in Figure 4 (A_{RMN}−D_{RMN}) is the low-intensity dispersive D-band, which appears with a maximum at 1277 cm^{-1} for the YAG laser excitation of 1064 nm which is utilized in our experiments. This feature is associated with disordered, sp^3-hybridized carbon present as impurities and SWNT defects.[54,55] For this reason, the ratio of the amplitudes of the G-band and the D-band has been used as a measure of the purity of AP-SWNT soot and to evaluate the efficiency of purification.[17] More recently, the spectral width of the D-band was suggested as an alternative measure of purity.[18] The majority of purity evaluations using Raman measurements of SWNT materials have made use of solid-phase SWNT samples in the form of powders, buckypapers, thin films, or individual SWNTs on substrates.

As can be seen in the middle panel of Figure 4, the intensities of the RBM- and G-bands for SWNT samples made with a range of Ni catalyst concentrations correlate with the AP-SWNT soot purities determined by NIR spectroscopy, reaching a maximum for sample C at 4 atom % Ni and declining for higher and lower Ni concentration. This qualitative correlation suggests that both NIR and Raman spectroscopy can be successfully used for purity evaluation. In obtaining the set of Raman spectra in Figure 4 (middle panel), we used the same dispersions of AP-SWNT soot in DMF as were employed in the NIR spectroscopy experiments (concentration of 0.01 mg/mL). The SWNT dispersions were placed in 5 mm diameter NMR sample tubes for Raman study, and the solvent contribution was subtracted from the spectra.

To test the reproducibility of the purity measurements by NIR and Raman spectroscopy, we prepared five independent 50 mg probe samples from the same mechanically homogenized 10 g batch of AP-SWNT material. The recommended homogenization procedure, which includes several dilution−ultrasonication steps,[13] was used to obtain final 0.01 mg/mL dispersions for testing. The results of the NIR relative purity measurements are presented in Figure 7a. The five probe samples show an average relative purity of 46% with a standard deviation, SD, of 3.0%.

Figure 7b shows the area of the Raman G-band for the same five dispersed samples previously evaluated by NIR spectroscopy (Figure 7a). When normalized to the same average value as in Figure 7a, dispersion-phase Raman spectroscopy demonstrates a comparable scatter in the data with SD = 3.3%. Moreover, the sign and amplitude of deviation for each probe sample are remarkably similar for the NIR and Raman data in parts a and b of Figure 7, respectively, which shows that these two dispersion-phase analyses are essentially equivalent under these experimental conditions. Figure 7c represents the G-band areas and Figure 7d the ratios of the G-band area to the D-band area for the same five probe samples in dry powder form. Both of these plots show a significantly higher scatter with values spread between 34% and 64%, and it is clear that there are significant deviations from the normalized average value of 46%. The SD values for the experiments on dry powder samples are 3−5 times higher than for the solution-phase data (Figure 7b). Furthermore, we observed a similar scatter in the data by changing the position of the laser spot within a dry powder SWNT sample. Thus, solution-phase Raman spectroscopy provides much more reproducible results than for experiments conducted on solid samples, probably due to the higher degree of homogenization of the SWNT sample.

We now seek to define the most appropriate metric for a Raman spectroscopy-based purity evaluation, and to explore its relationship with the NIR relative purity measurement.[13] For this purpose we measured the Raman spectra of 15 AP-SWNT samples with NIR relative purities between 0 and 65%. We first tested the area of the G-band, because it shows very reproducible results (Figure 7b). Figure 8a gives the area of the G-band as a function of RP determined by the NIR technique.[13] From Figure 8a it is clear that these measures of Raman and NIR purity are directly proportional to one another; however, it is important to conduct the measurements at a constant SWNT concentration (we recommend 0.01 mg/mL). Thus, the G-band area is a good

(53) Rao, A. M.; Richter, E.; Bandow, S.; Chase, B.; Eklund, P. C.; Williams, K. A.; Fang, S.; Subbaswamy, K. R.; Menon, M.; Thess, A.; Smalley, R. E.; Dresselhaus, G.; Dresselhaus, M. *Science* **1997**, *275*, 187−191.
(54) Saito, R.; Dresselhaus, G.; Dresselhaus, M. S. *Physical Properties of Carbon Nanotubes*; Imperial College Press: Singapore, 1998.
(55) Dresselhaus, M. S.; Dresselhaus, G.; Jorio, A.; Souza Filsho, A. G.; Pimenta, M. A.; Saito, R. *Acc. Chem. Res.* **2002**, *35*, 1070−1078.
(56) Williams, K. A.; Tachibana, M.; Allen, J. L.; Grigorian, L.; Cheng, S.-C.; Fang, S. L.; Sumanasekera, G. U.; Loper, A. L.; Williams, J. H.; Eklund, P. C. *Chem. Phys. Lett.* **1999**, *310*, 31−37.

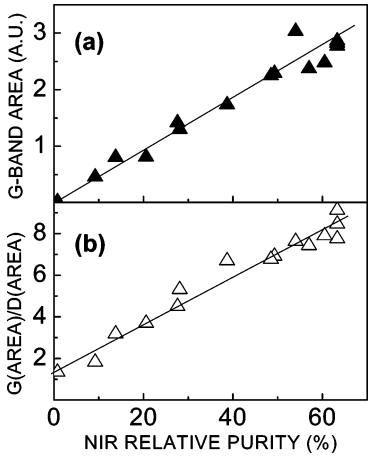

Figure 8. Correlation between purity evaluation criteria derived from solution-phase Raman and solution-phase NIR spectroscopy for 15 SWNT samples as a function of NIR relative purity: (a) Raman G-band area, (b) ratio of the areas of the Raman G- and D-bands.

candidate for a Raman metric of SWNT carbonaceous purity despite the fact that this mode is also present in the graphitic impurities, because the absence of resonant enhancement of this mode in graphite makes the per-carbon contribution from graphitic impurities significantly weaker than it is in the SWNT component.

As a second candidate for a Raman metric of purity, we measured the ratio of the areas of the G- and D-bands, and this figure of merit is presented in Figure 8b as a function of the NIR value. Clearly, there is a linear dependence, but the straight line which fits this relationship does not pass through the origin. The offset may be related to the fact that the G-band is also present in graphitic impurities, as discussed above, and thus, this contribution becomes more important for SWNT samples of low purity.

Thus, both of the Raman figures of merit evaluated above are potentially suitable for purity evaluation, and both correlate with the NIR relative purity (Figure 8). The direct use of the area of the G band gives less scatter in the data, but it requires the preparation of samples of exactly the same concentrations. Such an evaluation is not satisfactory as a general method because there is no internal standard with which to correct for variations in the experimental conditions, and it would therefore be difficult to compare data obtained with different instruments which are likely to operate with nontransferable focusing and collection optics and detector response. The measurement of the ratio of the Raman G- and D-band areas provides the necessary internal standard, but the results show more scatter than the NIR measurements as a result of the small area of the D-band.

We previously recommended a concentration of 0.01 mg/mL for the SWNT purity evaluation;[13] higher SWNT concentrations are difficult to stabilize as nonscattering dispersions, while reducing the concentration decreases the signal-to-noise ratio of the NIR and Raman spectra. To evaluate the importance of the SWNT concentration for NIR and Raman spectroscopy-based purity evaluation techniques, we prepared a series of dispersions of AP-SWNTs with concentrations between 0.05 and 0.001 mg/mL. Figure 9 shows the NIR relative purities obtained from the NIR spectra shown in the inset, as a function of SWNT concentration.

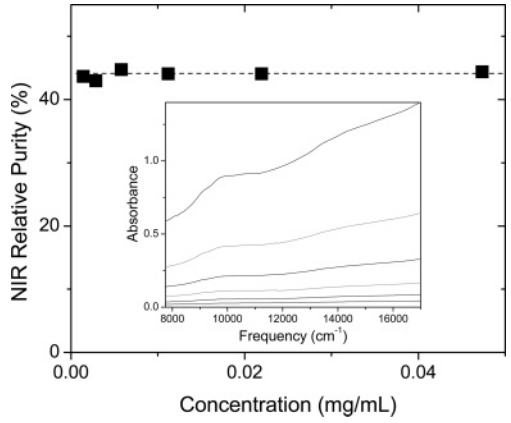

Figure 9. NIR relative purity as a function of the concentration of the SWNT dispersion. The inset shows experimental NIR solution-phase spectra utilized for calculation of purity.

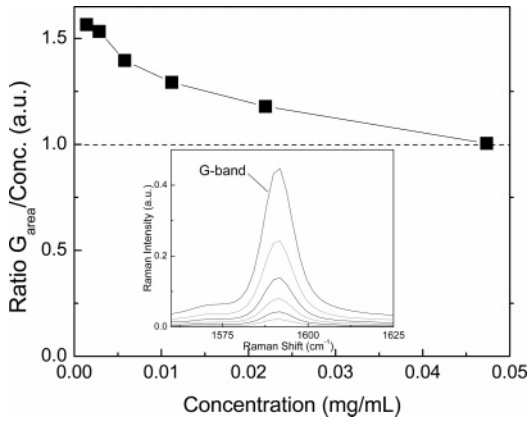

Figure 10. Area of the SWNT Raman G-band normalized to the concentration as a function of SWNT concentration. The inset shows experimental Raman spectra of samples used in the calculation.

Figure 9 demonstrates that the NIR relative purity values are independent of the SWNT concentrations, which is a simple consequence of the applicability of the Beers law to SWNT dispersions.[47] This confirms that relative purities determined by the NIR technique are internally consistent, and the sample preparation procedure does not require the exact matching of concentrations.[13,21,47]

The same series of SWNT dispersions was then studied using Raman spectroscopy, and the G-band regions of the Raman spectra are presented in Figure 10 (inset); as noted previously, the area of the G-band provides the most accurate evaluation of purity in the case of Raman spectroscopy (Figures 7b and 8a). However, Figure 10 shows that the ratio of the area of the G-band to the concentration is not a constant and increases at low concentrations. This dependence is presumably associated with the fact that, for solution-phase samples, Raman scattering does not occur on the surface of the sample, but in the 1−3 mm depth of the SWNT dispersion defined by the focusing conditions. In this situation, after initial Raman scattering the photons may undergo secondary scattering or absorption on their way out of the dispersion to the detector, thus reducing the strength of the Raman signal. This reduction in the Raman response will be enhanced with increasing SWNT concentration, and this explains the concentration dependence observed in Figure 10. Thus, matching the concentrations of the samples is

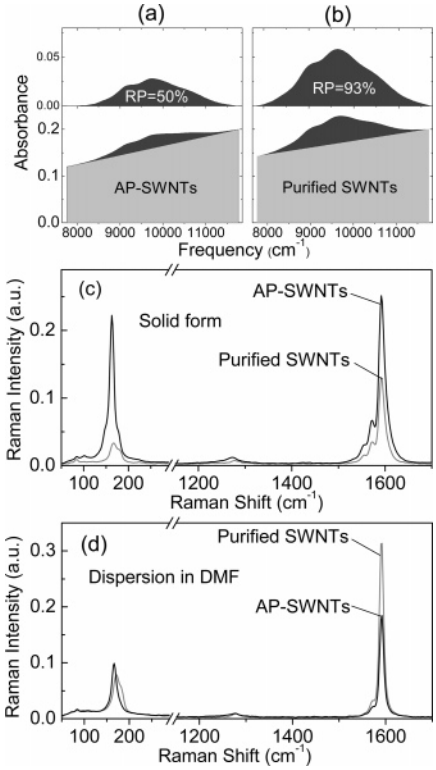

Figure 11. NIR spectra in the range of the SWNT S_{22} interband transition for (a) an as-prepared sample (NIR RP = 50%) and (b) a purified (NIR RP = 93%) sample (bottom panel, full spectra; top panel, S_{22} band after linear baseline subtraction). (c) Solid-phase Raman spectra of as-prepared (black line) and purified (gray line) SWNT samples. Note that the Raman signal of the purified solid sample is suppressed in comparison with that of the as-prepared material. (d) Solution-phase Raman spectra of as-prepared (black line) and purified (gray line) SWNT samples.

essential for the G-band area Raman spectroscopy-based purity evaluation technique.

An important purpose of a purity evaluation technique is the ability to efficiently monitor and optimize the parameters of a purification process.[17,18,20,21,43] By using the NIR purity evaluation technique, we were able to understand and optimize the nitric acid-based SWNT purification procedure.[20] On the other hand, we found that in many cases the intensity of the Raman response does not directly reflect the purity of processed SWNT materials. We observed significant suppression of the Raman signal after certain purification steps, and we take up this point below. Parts a and b of Figure 11 show NIR absorption spectra of an AP-SWNT sample (NIR RP = 50%) and an SWNT sample purified by a standard combination of oxidation in air followed by subsequent treatment in hydrochloric acid.[57] According to the NIR evaluation procedure[13] the carbonaceous relative purity increased from 50% to 93% as a result of the purification (Figure 11a,b) and the amount of residual metal catalyst decreased from 30% to 8%, as determined by TGA.

Figure 11c shows the Raman spectra obtained from standard SWNT powder samples, and it is apparent that the purified material shows a significantly weaker response than the AP-SWNT sample.

Figure 11d gives the Raman spectra of the same DMF dispersions of as-prepared and purified samples, which were used in the NIR measurements (Figure 11a,b). In this case we observe a 1.7-fold increase in the area of the G-band as a result of the purification, in accord with the NIR measurements (Figure 11a,b), and the ratio of the areas of the G- and D-bands increased by the same factor. These data confirm that solution-phase Raman spectroscopy using the G-band area or the ratio of the areas of the G- and D-bands provides a much more reliable purity evaluation than data obtained from solid samples.

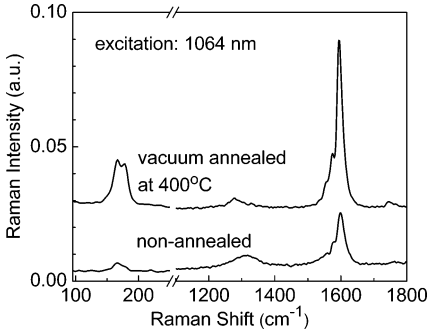

Figure 12. Raman spectra of an SWNT sample treated with nitric acid, before and after annealing at 400 °C in a vacuum.

The suppression of the Raman response is mainly due to the doping of the SWNT material during nitric acid treatment.[32] Figure 12 shows the Raman spectrum of a solid sample of SWNTs purified by nitric acid treatment.[10,20] The relative carbonaceous purity of this SWNT material is evaluated as 90% by NIR spectroscopy, but it shows a very weak Raman response. Annealing in a vacuum at 400 °C for 90 min considerably enhances the Raman response. The carbonaceous purity is not expected to be modified by annealing at such low temperatures, and the measured NIR purity in a DMF dispersion is invariant to this annealing step.

It is known that nitric acid treatment leaves the material in a partially doped state, which significantly reduces the resonant Raman response of the SWNTs by suppressing the strength of the electronic interband transitions[32] and decreasing the lifetime of the excited states. Annealing in a vacuum leads to the removal of the residual charge-transfer intercalants,[32,35,38] thereby dedoping the SWNTs and recovering the strength of the interband transitions and the resonant Raman response. In addition, the deintercalation process leads to a modification of interactions between the SWNTs in the bundles, and this may also affect the Raman response.[58,59] Although we cannot state with certainty why the two techniques respond differently to doping of the SWNTs, the most likely differentiator is the lifetime of the excited states, which is directly involved in the resonant enhancement of the Raman intensity but largely irrelevant in determining the intensity of S_{22} interband electronic transitions for lightly doped SWNTs.[13,32]

In practice we found that purity evaluations based on solution-phase NIR spectroscopy are less affected by doping than those using solid-phase Raman spectroscopy (Figures 11 and 12), and this may be a reflection of the dedoping that occurs on dispersion of SWNT samples in DMF, which leads to a recovery of the strength of the S_{22} interband electronic transition that is utilized in the NIR purity evaluation technique.

(57) Chiang, I. W.; Brinson, B. E.; Huang, A. Y.; Willis, P. A.; Bronikowski, M. J.; Margrave, J. L.; Smalley, R. E.; Hauge, R. H. *J. Phys. Chem. B* **2001**, *105*, 8297−8301.

(58) Kahn, D.; Lu, J. P. *Phys. Rev. B* **1999**, *60*, 6535−6540.

(59) Henrard, L.; Hernandez, E.; Bernier, P.; Rubio, A. *Phys. Rev. B* **1999**, *60*, R8521−R8524.

It is important to note that the Raman spectrum of SWNTs is strongly resonance enhanced: laser excitation at a particular wavelength does not necessarily excite all diameters and types of SWNTs in the bulk sample; only those SWNTs with interband transitions matching the energy of the laser excitation will be observed.[53−55] Multiple excitation wavelengths must be used to detect the full range of SWNTs that are present in the usual heterogeneous sample. However, NIR spectroscopy is nonselective, and SWNTs of all diameters and chiralities are detected. The NIR purity evaluation technique was initially developed for electric arc SWNTs produced with Ni/Y catalyst,[13,21] but it can be adjusted to SWNT material produced by most techniques, such as laser ablation and HiPco.[60] The catalytic vapor deposition (CVD) technique usually produces SWNTs with an extremely wide diameter distribution. As a result, interband transitions in such SWNT materials overlap, and this obscures the NIR spectral features. Raman spectroscopy does not require a narrow diameter distribution and was successfully used for CVD-grown SWNTs, but requires the use of multiple excitation wavelengths.

6. Conclusion

We have presented an evaluation of the capabilities of the most popular analytical techniques, such as SEM, TEM, TGA, and Raman and NIR spectroscopy, for the evaluation of the purity of bulk quantities of SWNT material. The most accurate purity evaluation is achieved by solution (dispersion) phase NIR spectroscopy using the area of the semiconducting S_{22} interband transition, and solution (dispersion) phase Raman spectroscopy using the area of the G-band or ratio of the areas of the G- and D-bands. Sample preparation and homogenization are critical steps in obtaining an accurate purity evaluation. SWNT samples prepared in the form of thin films or, especially, powders produce a much higher scatter in the data than samples prepared in the solution phase. The sensitivity of the Raman technique to doping and solution concentration and the resonant nature of the technique render it unsuitable for general application in the present context. The NIR technique is easily applied and relatively insensitive to chemical processing of the SWNTs and may be used to obtain a complete sample profile in a single experiment. Unfortunately, it is not yet possible to provide an absolute value of the purity of SWNTs, but it is expected that the widespread adoption of the NIR technique will soon produce samples which cannot be further purified and may thus be considered analytically pure. Based on current estimates, we expect analytically pure SWNT samples to be characterized by values of AA(S)/AA(T) $\sim$ 0.325, and RP $\sim$ 230%.

Acknowledgment. This research was supported by DOD/DARPA/DMEA under Award No. DMEA90-02-2-0216. Carbon Solutions, Inc. acknowledges NSF SBIR Phase I and Phase II Award No. DMI-0110221 from the Division of Design, Manufacture and Industrial Innovation and a DARPA Phase I SBIR administered by the U.S. Army Aviation and Missile Command (Award No. W31P4Q-04-C-R171).

JA043061W

(60) Zhao, B.; Itkis, M. E.; Niyogi, S.; Hu, H.; Perea, D.; Haddon, R. C. *J. Nanosci. Nanotechnol.* **2004**, *4*, 995−1004.